González-Gómez, P. A., Gómez-Hernández, J., Briongos, J. V. & Santana, D. (2017). Thermo-economic optimization of molten salt steam generators. *Energy Conversion and Management*, 146, pp. 228–243.

DOI: 10.1016/j.enconman.2017.05.027

Thermo-economic optimization of molten salt steam generators

P.A. González-Gómez[*1], J. Gómez-Hernández[1], J.V. Briongos[1], D. Santana[1$].

[1]Department of Thermal and Fluid Engineering.

University Carlos III of Madrid

Campus of Leganes, 28911 Madrid (Spain)

*Phone number: +34 916246032, Fax: +34 916249430, e-mail: **pegonzal@ing.uc3m.es**

Abstract

This paper presents a methodology to guide the design of heat exchangers for a steam generator in a solar power tower plant. The low terminal temperature difference, the high fluid temperatures and the high heat duty, compared to other typical shell and tube heat exchanger applications, made the design of the steam generator for molten-salt solar power towers a challenge from the thermomechanical point of view. Both the heat transfer and the thermal stress problems are considered to size the preheater, evaporator, superheater and reheater according to the TEMA standards and ASME Pressure Vessel code. An integral cost analysis on the steam generator design effects on the power plant performance reveals an extremely low value for the optimum evaporator pinch point temperature difference. Furthermore, an optimization using genetic algorithms is performed for each heat exchanger, which leads to economical and feasible designs.

A 110 MWe solar power tower plant is studied. Two configurations of the steam generator are proposed: with one or two trains of heat exchangers. The results show that the optimum pinch point temperature differences are very close to 2.6 ºC and 3 ºC for the steam generator with one and two trains, respectively. The proposed design of the steam generator consists of a U-shell type for superheater and reheater, a TEMA E shell forced circulation evaporator and a TEMA-F shell preheater. Also, the approach point temperature difference analysis is performed to avoid subcooled flow boiling in the preheater. An economic study to compare forced and natural circulation evaporator designs is carried out.

Key words: *Solar power tower plant; Steam generator; Heat exchanger design; Design optimization.*

Nomenclature

Abbreviations

B&W : Babcock and Wilcox.

CT : cold tank.

CSP : concentrating solar plants.

ESDU : engineering science data unit.

EV : evaporator.

FW : feed water.

GA : genetic algorithm.

HEN : heat exchanger network.

HP : high pressure.

HPT : high pressure turbine.

HRSG : heat recovery steam generator.

HTF : heat transfer fluid.

HT : hot tank.

Hx : heat exchanger.

LP : low pressure.

LPT : low pressure turbine.

MSEE : molten salt electric experiment.

OSV : onset of significant voids.

PH : preheater.

REC : receiver.

RH : reheater.

SAM : system advisor model.

SG : steam generator.

SH : superheater.

SPTP : solar power tower plant.

TAC : total annualized cost (€/year).

TES : thermal energy storage.

Symbols

A : heat transfer area (m^2).

B_c : baffle cut (-).

C : cost (€).

Cp : specific heat capacity (J/kg ºC).

D : diameter (m).

H_y : annual plant operation time (h/year).

K : resistance coefficient (-).

L : length (m).

L_{bc} : baffle spacing (m).

L_{tp} : tube pitch (mm).

N_b : number of baffles (-).

N_{hot} : number of hot starts.

N_{warm} : number of warm starts.

N_{tp} : number of tube passes (-).

N_{tt} : number of tubes (-).

N_s : number of shells (-).

P : pressure (Pa).

Q : heat (W).

R : fouling resistance (ºC m^2/W).

$R_{\min}$: U-tube minimal radius (mm).

S : stream flow area (m^2).

T : temperature (ºC).

U : global heat transfer coefficient (W/m^2 ºC).

W : weight (kg).

h : convective coefficient (W/ m^2 ºC) or .

i : specific enthalpy (J/kg).

l_{ts} : tubesheet thickness (mm).

$\dot{m}$: mass flow rate (kg/s).

pc : penalty coefficient (-).

q_w : local heat flux (W/m^2).

t_s : shell thickness (m).

v : velocity (m/s).

$\mathbf{x}$: vector of optimization variables (-).

$\mathbf{y}$: vector of feasible constraints (-).

Greek Symbols

ΔS_{h-c} : hot and cold leg overhand difference (mm).

η : efficiency (-).

θ_{tp} : tube layout (º).

ρ : density (kg/m^3).

ϕ_v : viscosity correction factor (-).

Subscripts

dc : downcomer.

r : riser.

s : shell.

sat : saturated.

sub : subcooled.

t : tube.

ti : inside of tube.

w : window zone

x : cross-flow zone.

1. Introduction.

Commercial concentrating solar plants normally include an indirect steam generator (SG) system in which the energy is transferred by means of a heat transfer fluid (HTF) to produce steam. Typically, a SG includes four heat exchangers: superheater, reheater, evaporator and preheater. Additionally, the SG includes the steam drum, feed-water pumps, hot salt pumps and supporting systems. A conventional shell

and tube heat exchangers are normally selected for the SG. The intermittent operation conditions, the high working temperatures and the large mass flow rates associated present significant issues for heat exchanger designers.

Different studies for the design of molten-salt SGs of solar power tower plants (SPTPs) are available in the literature. The design requirements consider the material selection, geometric parameters and overall performance [1]. Other design guidelines also include the economical evaluation of the SG [2]. In both cases, these design recommendations analyze the SG design for a 100 MWe commercial SPTP. In spite of Foster Wheeler recommendations [1], a different approach is accomplished for the SG design of the experimental facility Solar Two [3] and Molten Salt Electric Experiment (MSEE) [4], showing that the SG design is a wide open research field.

The SG design depends also on the manufacturer. In this sense, several SG solutions proposed by different manufacturers were analyzed for a 100MWe commercial solar power plant in [2]. For instance, ABB Lummus [2] design includes a kettle evaporator and U-tube/straight shell heat exchangers. The salt is placed on the shell side in the superheater and preheater, whereas in the reheater the salt is placed on the tube-side. The superheater design is divided into two shells in series in order to decrease the thermal stress in the tubesheet. The SG design proposed by ABB Lummus presents the lowest cost compared to other manufactures. Struthers Wells [2] uses the same concept as ABB Lummus employing a kettle evaporator and U-tube/straight shell heat exchangers. The principal feature of this design is that the high-pressure water is placed on the shell side in all heat exchangers. This leads to high thicknesses, and thus, high thermal inertia. On the other hand, Foster Wheeler [1,2] proposes a straight tube/straight shell design with the molten salt placed on the shell side. In this design, the inlet and outlet streams pass through different tubesheets, avoiding the potential temperature gradients in the no-tube passes zone. The differential thermal expansion is accommodated by floating tubesheets. Furthermore, a natural circulation design is selected for the evaporator. The design proposed by Babcock and Wilcox (B&W) [2] consists of U-tube/U-shell heat exchangers with the molten salt placed on the shell side. Similarly to the straight tube/straight shell design, the U-shell design also avoids temperature gradients produced by inlet and outlet streams. In addition, the U-shaped tubes can expand or contract in response to the thermal expansion between tubes and shell without the need of floating tubesheets. The main disadvantage is that the U-shell design presents relative high costs. A forced circulation evaporator is selected instead of natural circulation evaporator.

In spite of these useful recommendations shown in [2], several design parameters such as velocities, pressure drops or tube diameters of the heat exchangers are missing. Nevertheless, these recommendations were used for the SG design of the experimental facility Solar Two [3]. Some problems appeared in Solar Two. On the one hand, problems related to the stress corrosion materials appeared in such facility. For this reason, higher corrosion resistance materials for SG have been recommend by different authors [5,6]. On the other hand, further problems related to the salt freeze inside of the tubes of the kettle evaporator occurred in Solar Two [7], pointing out the difficulties found in the industry to design and operate SG systems.

Most recent studies have been made for higher SPTPs capacities where a prelaminar SG design can be found. Kolb [8] carried out a study to increase the efficiency of these plants. The SG sizing for 160 MWe subcritical and supercritical steam-cycles was calculated including the associated heat transfer areas and pressure drops. Kelly [9] proposed different strategies to reduce the levelized cost of electricity using supercritical heat transport fluids for central receiver power plants. The sizing and cost analysis of subcritical and supercritical SGs for 400 MWe plants were also studied.

Recently, genetic algorithms (GA) have been used extensively as an optimization method in the heat exchanger design. For instance, Caputo et al. [10] and Sadeghzadehet al. [11] performed a cost design optimization of shell and tube heat exchanger using GA. Their results show significant cost reductions over heat exchangers designed using traditional methods. Hajabdollahi et al. [12] used both GA and particle swarm method to optimize the cost of a shell and tube heat exchanger condenser. They claim that GA provides lower CPU time compared to particle swarm method. González-Gómez et al. [13] carried out the optimization of heat exchangers of parabolic trough solar power plant. Two optimization strategies were compared: minimize the heat transfer area and minimize the total annualized cost, considering capital and operation costs. Their results show that the minimization of the total annualized cost may lead to lower costs.

In this is work, a complete methodology for the design of SG for a SPTP is proposed. This approach considers the general requirements of the SG heat exchangers (superheater, reheater, evaporator, preheater and drum), the materials selection, the thermal-hydraulic and the mechanical designs together with the cost models and an optimization procedure. To accomplish such work, once the general requirements are satisfied, the approach consists of finding the optimum value of the pinch point

temperature difference of the SG. An approach point temperature analysis is made to avoid subcooled flow boiling in the preheater in order to use low cost materials. The optimization of each heat exchanger is carried out employing a genetic algorithm [13], while the overall cost is optimized studying the whole SG.

2. Initial design of SPTP.

The SPTP analyzed for the SG optimization is Crescent Dunes [14], which consists in a 110 MWe plant with 3.8 solar multiple and 10 storage hours. These features allow to obtain a 52% capacity factor. A simplified schematic of the different subsystems of the plant is shown Fig.1. The solar field is composed by heliostats following a radial staggered arrangement, which reflect the solar radiation into a receiver. The heat transfer fluid employed is molten-salt, which is heated from around 290 to 565ºC in the receiver. The thermal energy storage (TES) system is formed by two tanks (one hot and one cold) allowing the controlled release of the thermal energy captured from the solar field. The steam generator (SG) system includes a superheater (SH), reheater (RH), evaporator (EV) and preheater (PH). The hot salt is sent to SG where the thermal energy is transferred to produce main and reheated steam. The power block consists of a subcritical Rankine-cycle with a regenerative system. The main steam pressure and temperature are 12.6 MPa and 550ºC, respectively; and its efficiency is 44%. The main design values of the power block are summarized in Table 1. The water and steam properties are calculated using the correlations published in [15]. The molten-salt properties are obtained from [16].

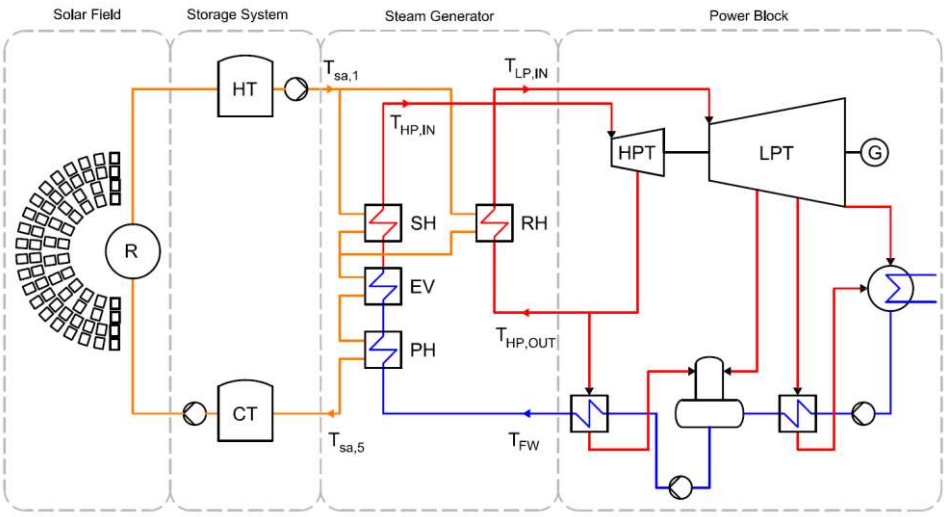

Fig. 1 Schematic of a SPTP.

Table 1
Nominal values of the 110 MWe steam power cycle.

Turbine point	Pressure (MPa)	Temperature (ºC)	Mass Flow (kg/s)
HP in	12.6	550	86.92
HP out	3.4	371	78.70
LP in	*	550	78.70
Feed-Water	*	245	86.92

*These parameters are subjected to SG design calculations.

3 Methodology

This section describes the procedure followed to design individually each heat exchanger of the SG. First, an initial design that follows the technical requirements and recommendations is proposed. After that, the materials, the thermal-hydraulic conditions and the mechanical design are analyzed. Fig. 2 shows a simplified scheme of the approach, which is further detailed in this section. Later, a global economic optimization of the SG is carried out using GA and costs models.

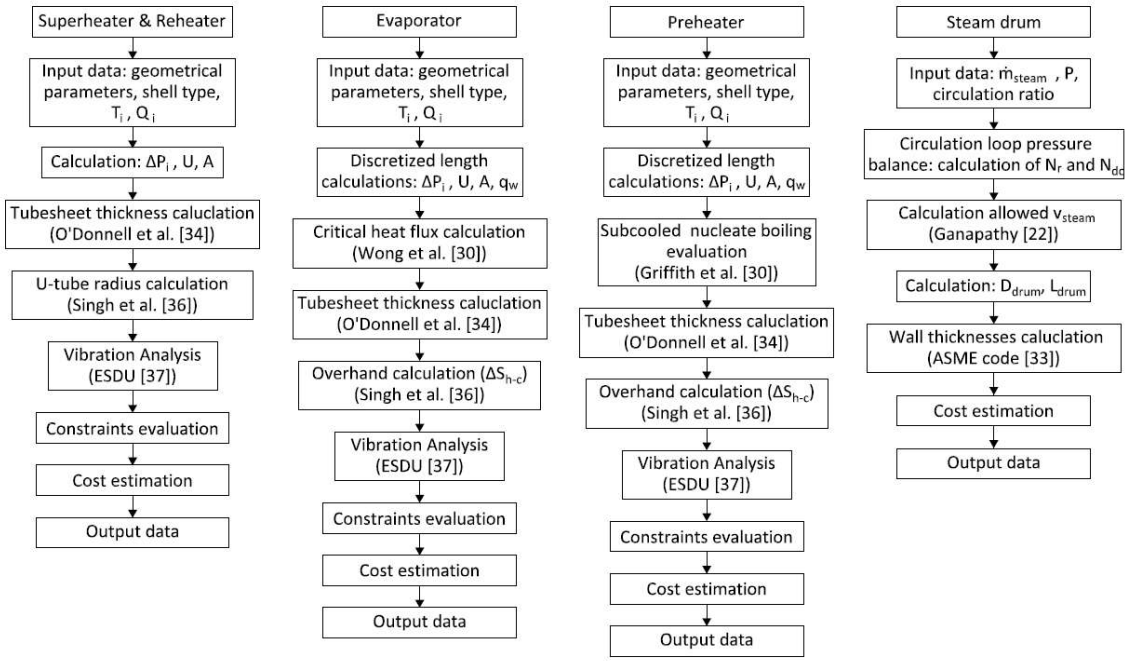

Fig. 2 Schematic of the main heat exchanger calculations.

3.1. SG design selection.

A general problem in the heat exchangers of the SG is the differential thermal expansion between the shell and the tubes. This is caused by the high temperature differences between the inlet and the outlet of the working fluids. Then, the different temperature profile of the working fluids leads to different thermal expansion in the shell and the tubes. To solve that, two designs are normally used: U-tube or floating head. The floating head design presents higher costs than U-tube mainly for two reasons: i) higher capital

cost [17]; ii) higher cost associated to maintenance [2]. Therefore, in this work a U-tube design is selected for all heat exchangers of the SG.

Since solar plants are subjected to daily transient operations, the reduction of the thicknesses of the heat exchangers may improve dynamic behavior of the SG against thermal stresses. Therefore, low-pressure salt is placed on the shell-side and the high-pressure water/steam on the tube-side.

3.1.1. Superheater and reheater requirements.

The main technical problem of the superheater is the high temperature differences between the inlet and outlet of the steam (~200ºC). This may lead to high temperature gradients in a single-tubesheet design, especially in the no-tube-lane zone. Furthermore, the temperature profile in the superheater produces a high differential thermal expansion of the hot leg over the cold leg of the tube bundle. This may involve a high curvature radius in the U-bend and thus an increase in the associated shell diameter. The U-shell design provides a good solution to solve the aforementioned problems since it has two tubesheets, and then, the thermal stresses produced in the no-tube-lane zone are eliminated. Moreover, in this design, a high U-bend radius does not lead to a high shell diameter. This design was employed successfully in the experimental facility MSEE [4].

The technical problems described in the superheater also occur in the reheater, although the working pressure in the reheater is considerably lower. Finally, an U-shell design is selected for the superheater and the reheater.

3.1.2. Evaporator requirements.

Several studies of parabolic trough plants include a kettle evaporator for the SG due to its relatively low capital cost and its successful operation in the pioneering CSP plants, such as in Luz Solar Electric Generating Stations (80 MWe) [2]. Nevertheless, the breakage of tubes in a kettle evaporator in Solar Two experimental facility due to the salt freeze-thaw cycling warns against its application [7]. For this reason, in this work a circulation evaporator type with steam drum was selected for the SG.

Mainly two designs are possible for circulation evaporators: forced or natural. According to Pasha [18], heat recovery steam generators (HRSGs) with forced circulation systems have shorter start-up times than natural circulation systems. This is because the natural circulation systems need enough driving pressure

to assure natural circulation, which may lead to a high thermal inertia. In addition, in forced circulation evaporators the circulation ratio is not dependent on the heat abortion. Thus a lower time is required to achieve the optimal circulation. For these reasons, forced circulation evaporators may provide advantages for plant operability. Normally, in HRSGs with forced circulation systems the circulation ratio is ranged between 3 and 8 [19], whereas in natural circulation systems is ranged between 8 and 25 [18].

In spite of the aforementioned advantages of the forced circulation design, it is not clear what design provides lower costs, in terms of capital investment and operation. Therefore, in this work a cost analysis is carried out to help in the selection of the best design. The pump operating costs on tube-side and shell-side, the capital cost associated to the heat exchangers and the start-up energy cost are considered. The proposed designs for forced and natural circulation evaporators are illustrated in Fig. 3-a and Fig. 3-b, respectively.

Different assumptions are made for the calculations. The number of downcomers and risers is calculated to fulfill the maximum momentum according to [1]. The maximum diameters are set to 450 mm and 150 mm, respectively. In the natural circulation design, the downcomer height is adjusted to provide the specified circulation ratio. In both designs, the tube length is discretized at least to the baffle spacing, to obtain accurate values for the two phase flow calculations (heat transfer coefficient, pressure drop, heat flux, etc.). Details of the evaporator calculations are described in Appendix A.

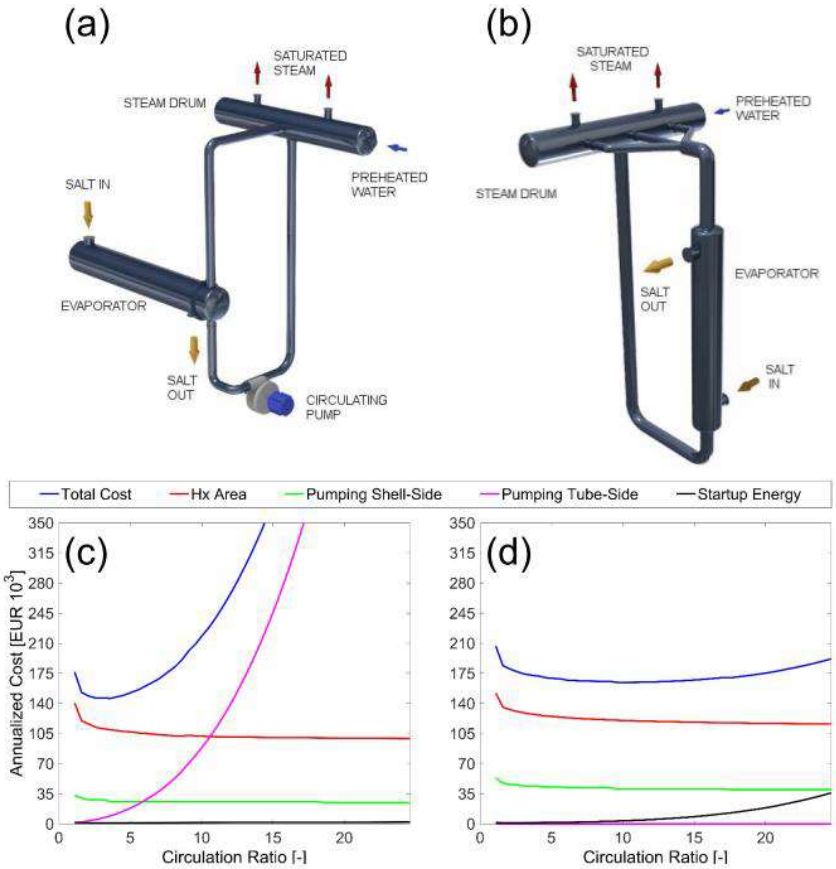

Fig. 3 Evaporator design: a) Forced circulation evaporator. b) Natural circulation evaporator. The annualized cost against the circulation ratio: c) Forced circulation evaporator; d) Natural circulation evaporator.

As can be seen in Fig. 3-c and Fig. 3-d forced circulation evaporator provides lower costs. Although both options include an economical straight shell design, the forced circulation design also allows a horizontal orientation to use a U-tube rear-end type and then reduce the heat exchanger costs. In contrast, natural circulation design requires a floating head type increasing the heat exchanger cost.

Different TEMA shell types such H or F are possible solutions as heat exchanger in a horizontal circulation evaporators [20], but finally a TEMA E shell is selected for different reasons. Firstly, TEMA E shell type is one of the most economical and the most common shell designs. Secondly, the inlet salt nozzle can be moved at the bottom of the heat exchanger, reducing the potential thermal stress in the tubesheet. In addition, the thermal stress in the U-tube rear-end type is also reduced since the differential thermal expansion between cold and hot legs is minimized.

3.1.3. Preheater requirements.

The preheater do not have a high temperature differences between inlet/outlet on the salt and water sides (around 50ºC and 70 ºC, respectively), therefore a single-tubesheet design is a feasible and economical

option. This solution was used in the experimental facility Solar Two without technical issues [3]. Moreover, the pinch point and the approach point temperature differences (Fig. 4) reported in the literature are typically low, and then, high thermal effectiveness will be required. For these reasons, a TEMA F shell is selected for the preheater.

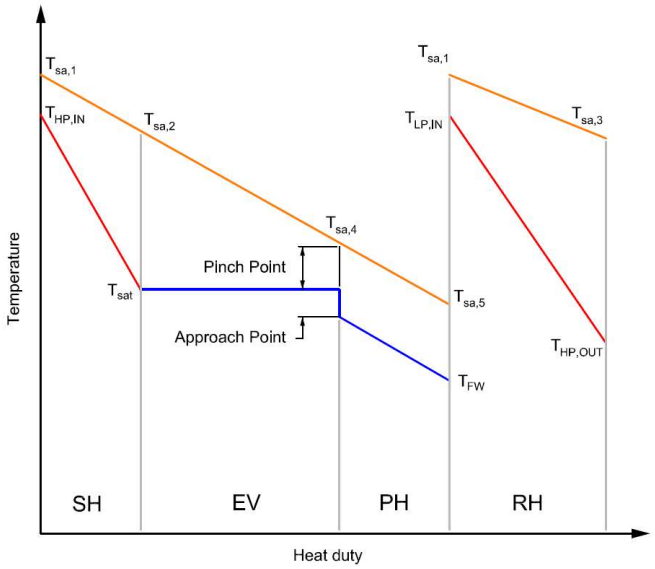

Fig. 4. Typical temperature profile for the SG.

Typically, in conventional fossil-fired plants and HRSGs, an approach point temperature difference between exit water of the economizer and the saturated water of the steam drum is imposed to prevent generation of steam in last zone of the economizer; this phenomenon is called steaming or subcooled flow boiling. The steaming may lead to vibrations and mechanical damage by water hammer [21], which can produce a fast deterioration of the economizer, unless a steaming economizer is used. The approach point temperature difference depends on the manufacturers and technologies. For instance, in conventional fossil-fired this temperature difference shows values of 15-25 ºC and in HRSGs ranges from 5 to 35 ºC [22]. For molten salt steam generators, the approach point used by ABB Lummus, Struthers Wells and Foster Wheeler was 0 ºC, in contrast, B&W chose 1.5 ºC [2].

3.1.4. Drum Requeriments.

The steam drum size is estimated assuring that the vertical and horizontal steam velocities are below the values recommended by Ganapathy [23]. This is important to achieve a proper operation of the chevron ensuring that the water droplets are not dragged by the steam flow.

Finally, Fig. 5 shows the heat exchanger configuration selected for the SG.

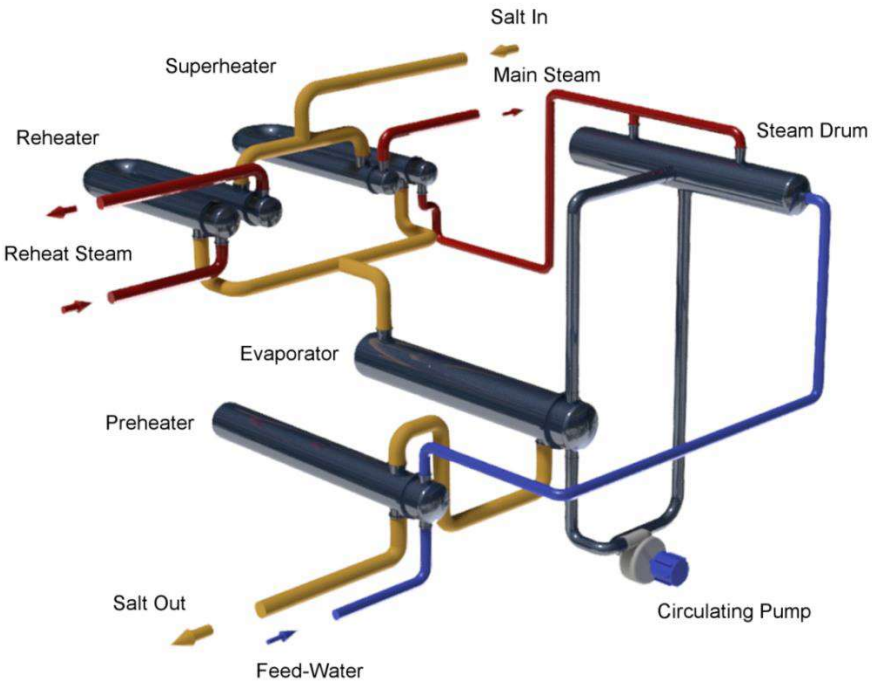

Fig. 5 Heat exchanger configuration selected for the SG.

3.2. Material Selection.

Zavoico [5] recommends the materials for different parts of the SG: Gr 347 or 321 stainless steel for the superheater, 9Cr-1Mo alloy steel for evaporator and carbon steel for preheater. For the superheater and the reheater, a lower cost stainless steel such as 304 or 316 are recommended by several manufacturers [2]. In contrast, according to Kelly [7], 304 or 316 stainless steel may be susceptible to stress corrosion cracking because of the potential impurities in the industrial-grade molten-salt used. For the preheater and the evaporator, in a first step, Zavoico [5] recommended materials were selected. Finally, in order to decrease the thermal stress on the U-bend zone, the selected tube materials are ASTM A210, Gr. A1 for preheater and ASTM A213, Gr. 347 for evaporator. The materials selected for the SG are shown in Table 2.

Table 2
Selected Materials for the main SG components.

Component	Shell and Tubesheet Material	Tube Material
Preheater	A516, Gr. 70	A210, Gr. A1
Evaporator	A387, Gr. 91	A213, Gr. 347
Superheater	A240, Gr. 347	A213, Gr. 347
Reheater	A240, Gr. 347	A213, Gr. 347
Steam Drum	A516, Gr. 70	-

3.3. Thermal-Hydraulic Design.

The sizing of the SG heat exchangers is carried to fulfill the heat duty requirements, which are specified by the power block. A computer code is performed to calculate several geometric parameters of the heat exchangers.

The shell-side pressure drop is calculated based on the stream analysis method using the Wills-Johnston version [24]. This method consists in a hydraulic network, where the shell-side flow is divided into six different streams: the tube-to-baffle leakage (A), the cross-flow (B), the bundle-to-shell bypass (C), the shell-to-baffle leakage (E) and the tube-pass-partition by-pass (F). The pressure drop per baffle is calculated using Equation (1). This equation is solved by an iterative process where the convergence is achieved when the same pressure drop is obtained in the meeting points of the different paths.

$$\Delta P_j = \frac{K_j (\dot{m}_j / S_j)^2}{2\rho\phi_v} \qquad j = A, B, C, E, F \tag{1}$$

At this point, the percentage of the different stream flows respect to the total flow is known, then the heat transfer coefficient on the shell-side can be estimated using the correlation proposed by Engineering Science Data Unit (ESDU) [25], which is expressed in terms of the heat transfer coefficients on cross-flow zone.

3.3.1. Double segmental baffle calculations.

In a first step, the heat exchanger design is carried out using single-segmental baffle, obtaining high shell side pressure drops. These optimized designs obtained in the first step tend to minimize the shell-side velocity to reduce the operational cost, in spite of the increment in the heat exchange area and the associated increment in the capital cost. For these reasons, a double-segmental baffle (Fig. 6) is selected providing a good option to reduce the pressure drop. In addition, double-segmental baffles may reduce the tube vibration, especially when larger mass flow rates are involved [26].

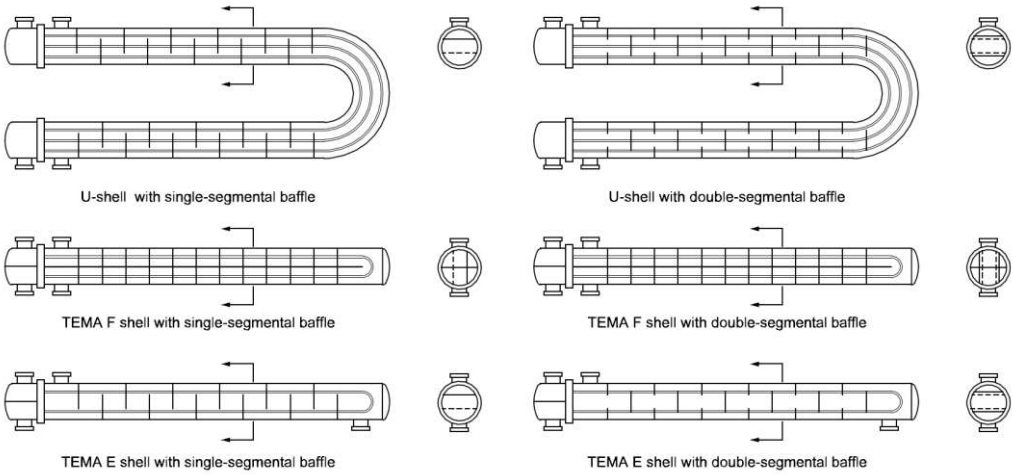

Fig. 6. Shell and baffle types.

The heat exchanger is divided in two symmetrical main streams to obtain the shell-side pressure drop in double-segmental baffles. Each one has their corresponding sub-streams mentioned before. Now, the ideal hydraulic network is solved adapting conveniently the flow areas of each sub-stream. A similar concept is used in the method proposed by K. P. Singh et al. [27] for triple-segmental baffles calculations. To validate this approximation, different designs reported in the literature were consulted [1,24]. The nozzle pressure drops are also considered in shell-side calculations.

According to ESDU [25] the heat transfer coefficient on the shell side can be estimated considering only the cross-flow in single-segmental baffles. In contrast, this consideration is not valid for double-segmental baffles since the percentage of parallel flow respect to the total flow may increase using double-segmental baffles, and it may lead to a reduction in the overall heat transfer. Then, the heat transfer coefficient on the shell-side is calculated using the Equation (2) proposed by Emerson [28]. This equation takes into account the heat transfer coefficients in the cross-flow and window zone, which are weighted by their respective heat transfer areas. The heat transfer coefficient in the cross-flow zone is calculated using the Colburn correlations [24]. The heat transfer coefficient on the window zone is calculated using the correlation proposed by Singh et al. [27].

$$h_s = \frac{A_x h_x + A_w h_w}{A_x + A_w} \tag{2}$$

3.3.2. Heat transfer and pressure drop inside tubes.

For single-phase flows, the heat transfer on the tube-side is estimated using Gnielinski correlation [24]. Since the heat exchangers are arranged horizontally, the pressure drops on the tube-side by static head losses are neglected. The friction factor is calculated using the Colebrook correlation [24]. The pressure drop for tube pass and the momentum change in nozzles are also taken into account.
For two-phase flows, the heat transfer coefficient is calculated according to Chen's correlation [29]. This correlation considers two heat transfer mechanisms: the nucleate boiling and the two-phase forced convection. The pressure drop for two-phase flows is calculated using the method proposed by Lockhart and Martinelli [24]. Two-phase effect in geometries such as bends and nozzles, have been also considered.

3.3.3. Critical heat flux calculation.

The critical heat flux is defined as the point which above the two-phase heat-transfer coefficient drops and takes place the departure of nucleate boiling phenomenon. Normally, the evaporators are not designed to operate near of the critical heat flux, not only for the decrease in the heat transfer coefficients but also to prevent the tube wall overheating. This problem appears when a zone in the evaporator exceeds the critical heat flux, showing an alternating process of dryout and wetting in the internal wall [30]. Therefore, cyclic thermal variations in the tube wall may lead to deposit-corrosion and fatigue damage. Moreover, this effect is related to flow instabilities that may reduce the performance.

The critical heat flux point mainly depends on the operating pressure, the mass velocity and the steam quality, the tube orientation, etc. To calculate the critical heat flux in horizontal tubes, the correlation proposed by Wong et al. [31] is used. Moreover, Collier et al. [30] recommends for boiling flows in horizontal tubes a minimum fluid velocity of 2.5 m/s in order to avoid steam water stratification problems.

Forced circulation evaporators require a careful economic study. As shown in Fig. 3 the optimal value of the circulation ratio is obtained around 2.5. However, the operation at the optimal circulation ratio exceeds the maximum heat flux allowed in the rear-end zone of the U-bend. Then, to operate the evaporator safely, a minimum circulation ratio of 5 is required. Other design employs multi-lead ribbed tubes in the evaporator which increases the steam quality working below of the critical heat flux conditions [4]. This means that the circulation ratio decreases, and then, the evaporator could be operated in the optimal economic performance. However, no correlations or experimental data about the critical

heat flux using multi-lead ribbed tubes were found, and thus, this design option has not been considered in our analysis.

3.3.4. Subcooled flow nucleate boiling.

Although, the preheater is designed to not overpass the saturation temperature of the steam drum, subcooled flow nucleate boiling may occur at local conditions. A correlation proposed by Griffith et al. [32], Equation (3), is used to estimate the local temperature difference at which starts the Onset of Significant Voids (OSV). Down-stream of this point, the void fraction increases rapidly. Therefore, it has been considered steaming conditions when the tube bulk temperature fulfills this condition:

$T_{t,bulk} \geq T_{sat} - \Delta T_{sub,OSV}$.

$$\Delta T_{sub,OSV} = q_w \frac{(14 + 0.1P_t)}{v_t} \tag{3}$$

A numerical model is performed to calculate the preheater local conditions (heat flux, wall temperature,…) following the method proposed by Hussaini et al. [33].

3.4. Mechanical Design.

Normally, a feasible heat exchanger is designed considering a high number of constraints. The standards of the Tubular Exchanger Manufactures Association (TEMA) [34] provide many geometrical constraints and design parameters such as: outside tube diameters, maximum and minimum baffle spacing, fouling resistances, clearances, etc. In this work, all heat exchangers are designed to fulfill these requirements. The thicknesses of heads, shells and tubes are calculated according to the ASME Boiler and Pressure Vessel code Sections VIII and II [35]. Other design constraints, which are based on good practice recommendations, are also used [13].

In order to reduce the cost associated to the tube-to-tubesheet welding and tube-support-plate drilling, the number of tubes is minimized [1]. In this way, the optimization algorithm penalizes solutions when the tube length is far from its maximum value.

3.4.1. Tubesheet thickness calculation.

Typically, the tubesheet thickness calculation in heat exchangers for standard industrial applications is carried out using ASME Section VIII-Division 1 or/and TEMA standards methods. However, these

methods do not consider the thermal stress effects in the U-tube tubesheet design. For this reason, more sophisticated methods were sought. The method proposed by O'Donnell et al. [36], considers the thermal stress and the stress produced by pressure. The thermal stresses are caused by temperature difference in the primary and secondary sides of the tubesheet, and in the no-tube-lane zone. Although in the standard industrial applications these effects are one or two orders of magnitude lower than the pressure stress, thermal stresses may become important when operating at high temperature differences, and thus, they should be combined with the pressure stress [37]. Then, to verify the heat exchanger designs on the safety-side, the O'Donnell method is used to calculate the tubesheet thickness. Fig. 7 illustrates the operating temperatures in the superheater tubesheet for different shell types. Details of the tubesheet stress calculations according to O'Donnell et al. [36] are described in Appendix B.

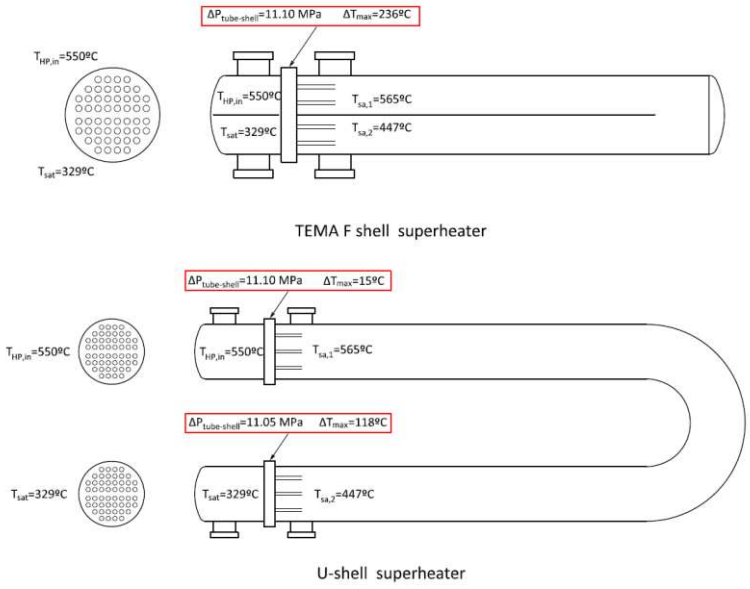

Fig. 7 Tubesheet temperatures for different superheater shell types.

3.4.2. Minimal U-tube radius calculation.

It is well known that the U-tube design avoids the thermal stress problem related to the differential thermal expansion between tubes and shell. Nevertheless, the thermal stress problem related to the differential thermal expansion between the hot leg and the cold leg is still present. The U-bend radius has a great influence on the thermal stress generated. Furthermore, since the tubes are supported by segmental baffles, the thermal expansion of the tubes is not free. Then, the tubes try to lose their straight shape and produce contacts at tubes and baffles located at the end of the U-bends, Fig. 8. Therefore, the location and the clearances of the last baffles play a key role on the generated stresses. In this work, the minimal

radius of the U-bend is calculated using the analytical method proposed by Singh et al. [38]. Fig. 9 shows the minimal radius against the temperature difference between the hot and the cold legs. The U-tube stress calculation according to Singh et al. [38] is described in Appendix C.

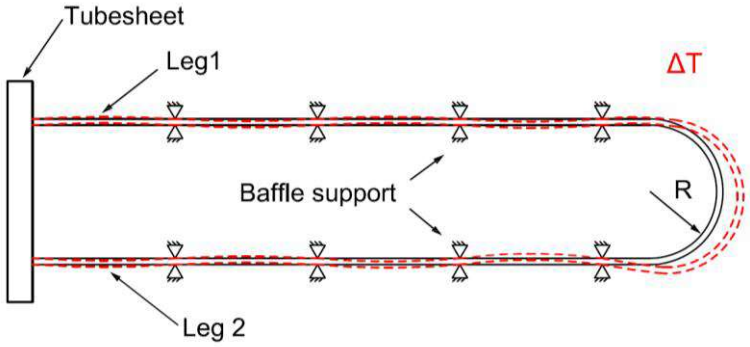

Fig. 8. U-tube deformation by thermal expansion.

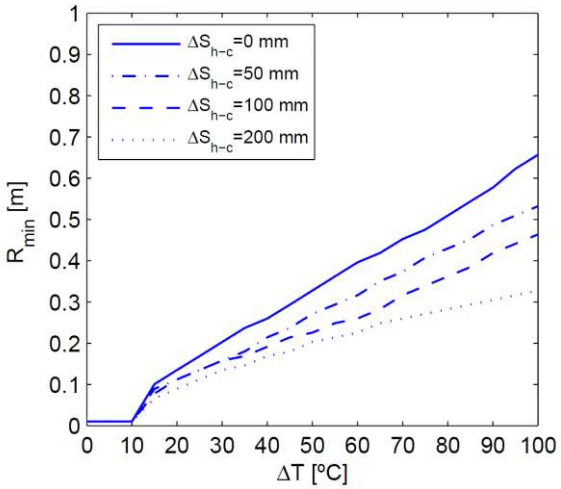

Fig. 9. Minimal radius against temperature difference between different hot and cold leg overhand differences (ΔS_{h-c}).

The minimal radius of the U-tube for the superheater and the reheater is calculated using a hot and cold leg overhand difference value of $\Delta S_{h-c} = 0$ in order to minimize the potential tube vibrations problems at the U-bend region. The U-tube radius for the evaporator and the preheater is selected according to the no-tube-lane distances reported in [39]. Then, the hot and cold leg overhand difference is adjusted below the maximum stress limit.

3.4.3. Vibration Analysis.

In the heat exchanger design high flow velocities lead to high heat transfer coefficients, obtaining in this way benefits such as low surface areas, cost, fouling tendency, etc. However, flow velocities above a

critical value can produce vibration problems, which cause the material erosion or even fatigue failure due to damage in tubes, baffles supports and tube-to-tubesheet joints.

A vibration analysis is performed for all heat exchangers using the method proposed by ESDU [40]. This method consists, in a first step, on finding the natural frequency of the tubes, which basically depends of the span length, the second moment of area of the tube and the densities of the shell and tube fluids. On second step, the critical velocity is calculated for a given tube layout.

3.5. Estimating Cost Models.

In general, the optimization of heat exchanger networks is considered as an isolated system. However, the operation of the SG in a SPTP affects the performance of the whole system. Therefore, it is convenient to evaluate the economic influence of each system.

The costs considered to evaluate SG are, on the one hand, the capital cost of the heat exchangers, the hot pump and the tank size of the TES system. On the other hand, the operational pump cost of the SG and the receiver. In addition, it is also considered the start-up energy cost. Finally, the total annualized cost (TAC) can be defined as:

$$TAC_1 = frc\ C_{capital} + C_{operation} \tag{4}$$

$$C_{capital} = C_{Hx} + C_{Pump} + C_{Tank} \tag{5}$$

$$C_{operation} = C_{pumping,REC} + C_{pumping,SG} + C_{start,SG} \tag{6}$$

The capital return factor (frc) is calculated considering an interest of 8%, a plant lifetime of 25 years and an annual insurance cost of 1%. The capital cost of the heat exchangers were estimated using the Purohit method [17]. This method takes into account many constructive parameters of the heat exchangers: front/shell and rear TEMA types, heat transfer area, tube layout, tube and shell side pressure, etc. Even cost factors for a wide variety of tube, shell, channel and tubesheet materials are also considered. However, the U-shell type cost factor is not available in this method. For this reason, an extrapolation is made according to the cost data from Foster Wheeler [1]. Since this method was developed in 1982, the heat exchanger costs must be escalated to the present value. According to Vengateson [41], the Chemical Engineering Plant Cost index can be applied for heat exchangers. The steam drum cost is calculated according Seider et al. [42].

The capital cost of the molten-salt pumps and tanks is estimated following the data provided by Kelly and Kearney [43]. The tank size can be calculated considering the storage hours and the molten-salt mass flow rate for the SG at nominal conditions. The costs of the molten-salt pumps, hot and cold, cost are calculated as a function of their required electrical power. The operational pump cost of the SG and the receiver is calculated using the Equation (7). The pump efficiency (η_{pump}) is considered to be 70%. The energy electricity cost (C_{power}) is assumed as 0.13 €/kWhe. Since the annual operating time of the SG ($H_{y,SG}$) is not known, it can be estimated by means of the solar plant capacity factor, obtaining 4550 hours.

$$C_{pumping,i} = C_{power} \frac{H_{y,i}}{\eta_{pump}} \left(\frac{\dot{m}_i \Delta P_i}{\rho_i} \right) \tag{7}$$

The annual operating time of the receiver ($H_{y,REC}$) is estimated using System Advisor Model (SAM) [16], obtaining 2970 hours. For simplification, it is assumed that the receiver operates at nominal conditions with an equivalent annual operating time of 2160 hours. The pressure drop in the receiver is estimated using the receiver modelling proposed by Rodríguez-Sánchez et al. [44].

The start-up energy is calculated using Equation (8). According to Foster Wheeler [1], the number of hot start-ups (N_{hot}) and warm start-ups (N_{warm}) are 300 and 10, respectively; the proposed cold-down rates of each heat exchanger are also used.

$$C_{start,SG} = C_{power} \left[\sum_{j=1}^{M} V_j \rho_j (N_{hot} \Delta i_{j,hot} + N_{warm} \Delta i_{j,warm}) + W_{hx}\, Cp_w (N_{hot} \Delta T_{hot} + N_{warm} \Delta T_{warm}) \right] \eta_{PB} \tag{8}$$

3.6. Heat exchanger Optimization using genetic algorithms.

Due to the high number of variables and constraints that involve the heat exchanger design, an optimization algorithm is employed to obtain a feasible and an economical design. Genetic algorithms are widely used because of their advantages, which are a relatively easy implementation and low computational cost. Moreover, the possibility of adding constraints and discrete and continuous variables makes these algorithms very attractive for the heat exchanger design. Further details of the GAs performance can be found in [11,45]. Here, the objective function is a combination of TAC and the penalty function, which are shown in Equations (9) and (10). The penalty function, Equation (11), is

defined according to Ponce et al. [46] to improve the performance of the algorithm. The main parameters for the GA implementation are the population size of 300 individuals, the crossover fraction of 0.8 and the mutation rate of 0.1. The maximum number of generations and the stall generation limit are set to 200 and 50, respectively. The search variables selected for the heat exchanger design are presented in Table 3.

Table 3
Search variables selected for the heat exchanger design.

Variable	Single-phase heat exchanger	Evaporator
x_1	Shell diameter	Shell diameter
x_2	Tube diameter	Tube diameter
x_3	Tube layout (triangular, square or rotated square)	Tube layout (triangular, square or rotated square)
x_4	Tube pitch	Tube pitch
x_5	Number of shells	Number of shells
x_6	Shell-side velocity	Shell-side velocity
x_7	Tube-side velocity	Tube-side velocity
x_8	Baffle cut	Baffle cut
x_9	Segmental baffle (single or double)	Circulation ratio

$$TAC_2 = frc\ C_{Hx} + C_{pumping,Hx} \tag{9}$$

$$fitness(\mathbf{x}) = TAC_2(\mathbf{x}) + penalty(\mathbf{x}) \tag{10}$$

$$penalty(\mathbf{x}) = \begin{cases} 0 & if\ \mathbf{x}\ is\ feasible \\ \sum_{i=1}^{N} pc_i\ y_i^2(\mathbf{x}) & otherwise \end{cases} \tag{11}$$

4. Optimization.

4.1. Optimization of the approach point of the SG.

In this work, an economic analysis is performed to compare the use of a steaming preheater and a non-steaming preheater. On the one hand, non-steaming preheaters show high approach point values that increase the log mean temperature, and therefore, the heat transfer areas and associated capital costs decrease. In addition, lower quality materials can be used. On the other hand, the heat transfer area of the evaporator increases since more steam must be generated to compensate the subcooled water temperature difference inlet at the steam drum.

In order to calculate the steaming conditions in the preheater, a finite difference scheme is performed using a tube length step of 0.1 m. The heat flux, the velocity and pressure are calculated at local conditions. Then, the Equation (3) is used to check if the steaming condition is achieved. If the steaming

condition is achieved at any point of the preheater, a steaming preheater is selected; otherwise a non-steaming preheater is selected.

4.2. Results of the approach point optimization.

The results of the approach point temperature difference analysis are shown in Fig. 10. A conventional salt temperature difference between inlet and outlet of the SG was selected (565 and 290 ºC, respectively) for this analysis. This means that the pinch point temperature difference is around 6.5 ºC for an approach point of 0 ºC. The results show that the steaming condition should not be achieved for approach points greater than 2.5 ºC. The abrupt change in the TAC is due to the higher cost materials used in the steaming preheater, which has been designed considering the same materials that has been used in the evaporator, Table 2. Furthermore, TAC shows a high growth rate for large approach point temperature differences. This means that the cost reduction due to the preheater area decrease does not compensate the cost increase in the evaporator using larger approach points.

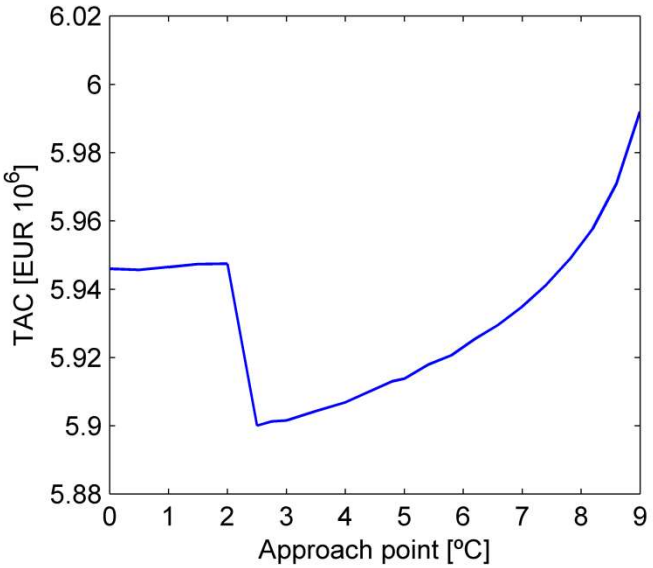

Fig. 10 Total annualized cost against approach point.

Regarding a different salt outlet temperature while keeping constant the inlet salt temperature to 565 ºC, different pinch points will be obtained, Fig. 4. Fig. 11 shows the minimum approach points for different pinch points at which the steaming conditions are not achieved, and then, non-steaming preheaters can be used. As can be seen in Fig. 11, the approach point increases with the pinch point. Large values of the pinch point reduce the heat transfer area needed due to the increase of the heat flux, and thus, the subcooled temperature difference increases too, Equation 3.

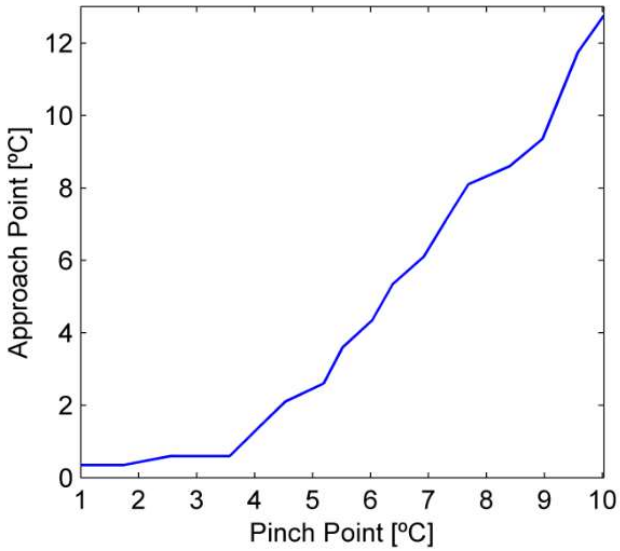

Fig. 11 Approach point against pinch point.

4.3. Optimization of the pinch point of the SG.

The pinch point optimization is a typical methodology used to evaluate the performance in systems such as HRSGs and heat exchanger networks (HENs) [47,48]. In this work, this methodology is used but a different approach is proposed for the SG design of SPTPs.

The pinch point is defined as the temperature difference between the inlet water evaporator temperature and the outlet salt evaporator temperature. The pinch point temperature difference has a high impact on the heat transfer areas of the SG, especially in the evaporator and the preheater. The pinch point also determines the salt mass flow rate and the outlet salt temperature of the SG. Then, low pinch point values may lead to large heat transfer areas, and therefore, high capital costs of the heat exchangers. Moreover, large heat transfer areas may also cause a high start-up energy consumption.

On the other hand, high pinch point values may increase the operational pump costs since high mass flow rate must circulate. This is very important because it affects: i) the SG pump energy consumption, ii) the receiver pump energy consumption, and iii) the storage tank size and its capital costs associated.

In this way, a trade-off between the mentioned costs may be obtained for a pinch point value that minimizes TAC. Fig. 12 shows a schematic of the evolution of the mentioned costs against the pinch point.

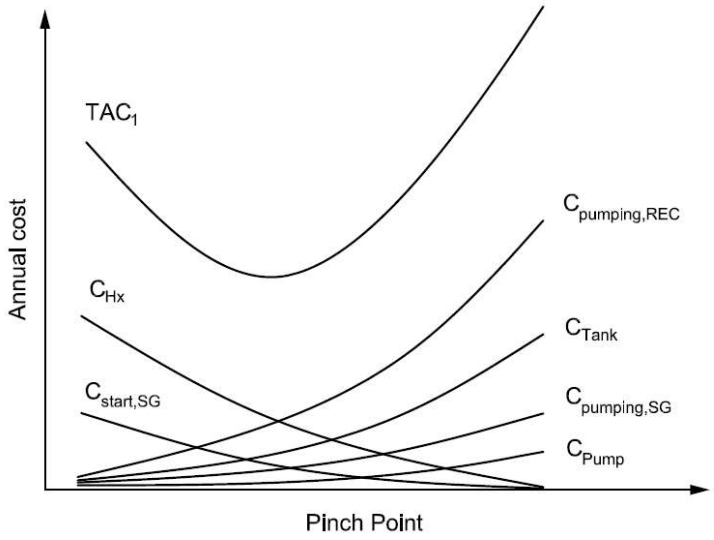

Fig. 12 Evolution of different costs against the pinch point.

4.4. Global optimization procedure.

The high number of possible combinations of the design variables of the four heat exchangers optimized simultaneously leads to a huge computational cost for the global optimization (around 10^{24} possible combinations). Therefore, an alternative method is proposed to reduce the number of the design variables and the computational cost.

The salt-side velocity has a very important effect in the total cost for different reasons. On the one hand, the thermal conductivity of the molten salt is lower than the water/steam. On the other hand, the shell-side velocities are normally lower than in the tube-side. Therefore, the overall heat transfer coefficient is dominated by the heat transfer on the salt side. This means that a high salt-side velocity reduces the heat transfer area, and then, decreases the capital cost. However, a high salt-side velocity increases the pressure drop and the associated operational costs. For these reasons, the salt-side velocity is selected as the main global design variable.

Bearing in mind that the heat exchanger optimization is made in a first step individually, this means that the GA minimizes TAC without considering the cost of other heat exchangers. In the second step, the whole system is considered in the global optimization algorithm. This algorithm can increase the salt-side velocity in the heat exchangers with higher capital costs (combination of the cost associated to the heat transfer area, material, shell type, …) or operate in the opposite form, changing the operating conditions of the cheapest heat exchangers. Then, the SH, RH, EV and PH are optimized simultaneously by means

of TAC_1, where the design variables are only the shell side velocities of each heat exchanger. A simplified scheme of the optimization algorithm is shown in Fig. 13.

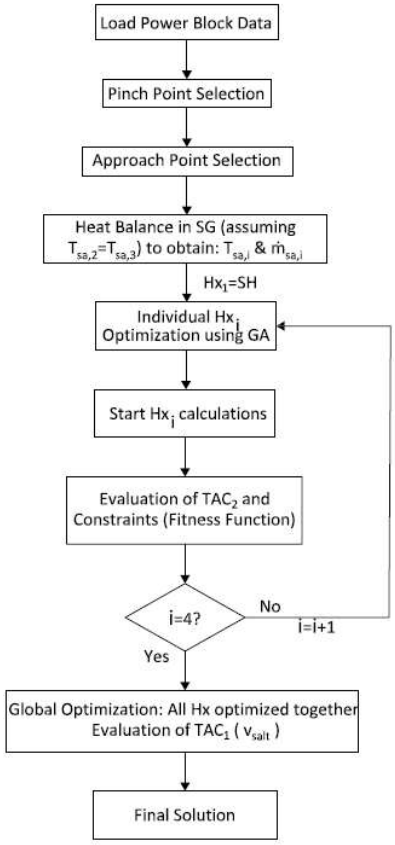

Fig. 13 Schematic of the optimization algorithm.

4.5. Results of the pinch point optimization.

In commercial solar power plants the SG is divided in two parallel trains [49,50]. This practice may reduce the stop time of the plant due to the potential failure risk of the SG. Although, initially it is not clear the advantages of a SG with two parallel trains, in this work a cost analysis is carried out for two different SG layouts: i) with only one train; ii) with two trains in parallel. A schematic of the SG layout with two trains is shown in Fig. 14. Each train is formed by superheater, reheater, evaporator and preheater.

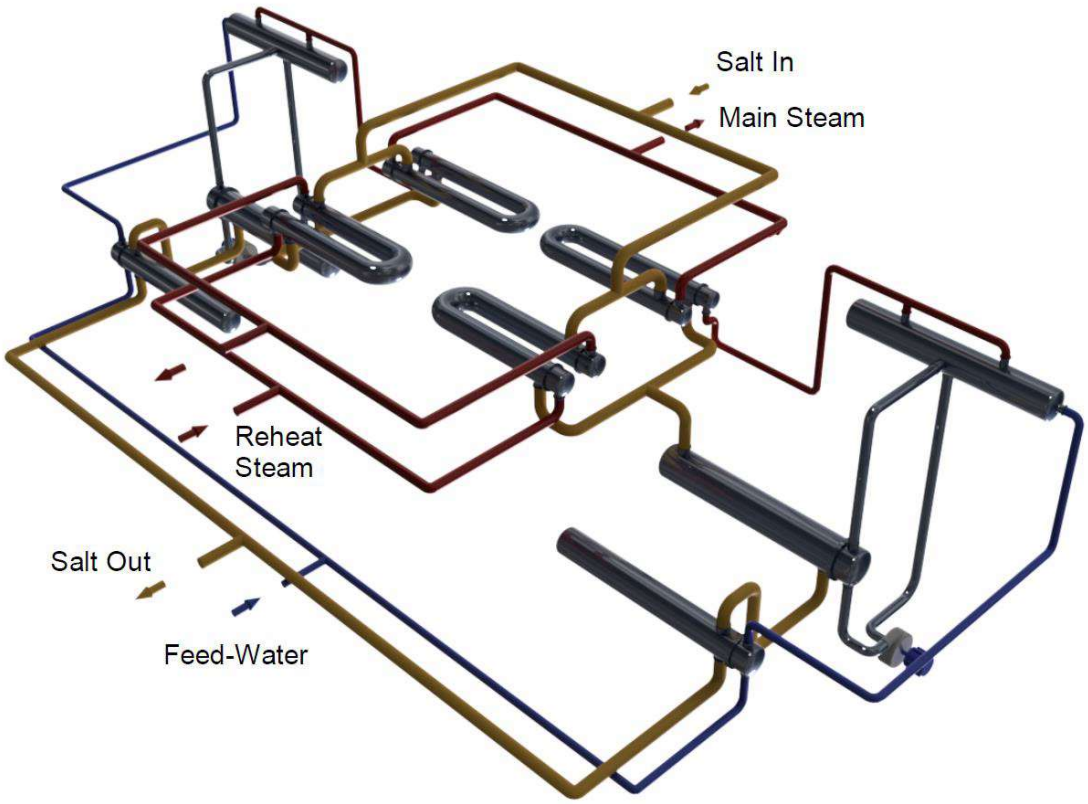

Fig.14 SG layout with two trains in parallel.

The pinch point optimization results for both SG layouts are illustrated Fig. 15. It can be seen that the minimum values of TAC corresponds to the optimum pinch points, which are 2.6 ºC and 3 ºC for the SG layouts with one and two trains, respectively. The SG with two trains has a higher TAC than the SG with one train due to the greater number of units used, i.e., heat exchangers, drums and pumps.

The optimal pinch points obtained are lower than the values suggested by the manufacturers, which range from 4.5 to 10 ºC [2]. This result can be explained due to the consideration in our model of the receiver pump operating costs, which are quite high. The results show that the optimal pinch points produces substantial savings compared to a value of 10 ºC (around 0.4 M€/year). In terms of temperature, a pinch point of 2.6 ºC causes a SG salt outlet temperature of 286 ºC, whereas a pinch point of 3 ºC produces a salt outlet temperature of 286.5 ºC.

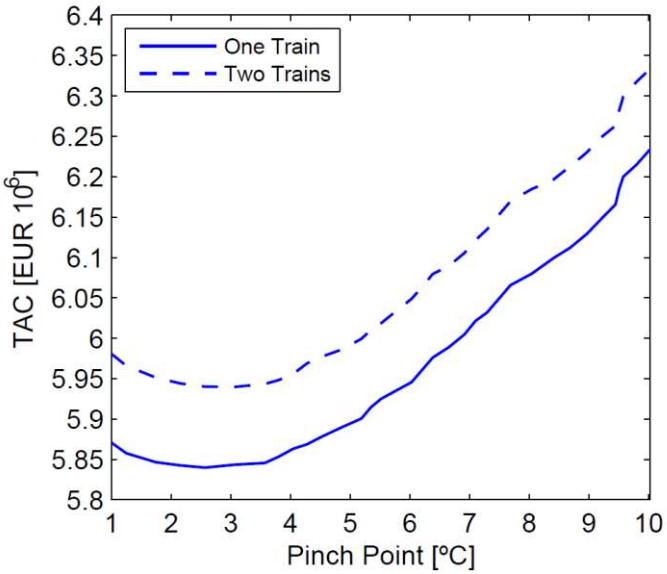

Fig. 15 Total annualized cost against pinch point.

4.8. SG proposed design.

The proposed designs of heat exchangers for the SG layouts with one and two trains are presented in Tables 4 and 5, respectively. These results are based on the pinch point optimization presented before. Several design parameters are included in the heat exchanger calculations. Also, the steam drum data of each SG layout is shown in Table 6.

Table 4

Proposed design of the heat exchangers for the SG layout with one train.

Parameter	Superheater	Reheater	Evaporator	Preheater
Shell diameter, D_s (mm)	884	1010	1796	1600
Baffle cut, B_c (%)	28	22	23	24
Baffle spacing, L_{bc} (mm)	612	317	569	658
Tubes ext. diameter, D_t (mm)	15.9	25.4	15.9	15.9
Tubes int. diameter, D_{ti} (mm)	12.2	21.2	12.2	12.2
Tube pitch, L_{tp} (mm)	20.7	31.8	20.7	23.9
Tube layout, θ_{tp} (º)	45	30	90	45
Tube passes, N_{tp} (-)	1	1	2	2
Tubes number, N_{tt} (-)	1219	815	2737-U	1615-U
Tube length, L_t (m)	20.81	22.09	9.43	11.04
Shell thickness, t_s (mm)	12.7	12.7	15.9	15.9
Tubesheet thickness, l_{ts} (mm)	254	193	400	312
U-tube minimal radius, R_{min} (mm)	395	713	42	48
Mass flow (tube-side), $\dot{m}_t$ (kg/s)	86.92	78.70	567.13	86.92
Mass flow (shell-side)), $\dot{m}_s$ (kg/s)	390.44	183.30	573.75	573.75
Flow velocity (tube-side), v_t (m/s)	13.21	23.96	2.53	0.61
Flow velocity (shell-side), v_s (m/s)	0.65	0.50	0.60	0.70
Convective heat transfer coefficient (tube-side), h_t (W/m^2 ºC)	3649	1227	27688	6598
Convective heat transfer coefficient (shell-side), h_s (W/m^2 ºC)	5213	3656	4200	4234
Fouling resistance (tube-side), R_t (ºC m^2/W)	8.825e-5	8.825e-5	2.647e-04	8.825e-5
Fouling resistance (shell-side), R_s (ºC m^2/W)	8.825e-5	8.825e-5	8.825e-5	8.825e-5
Overall heat transfer coefficient, U (W/m^2 ºC)	1241	664	1295	1448
Heat exchange area (per shell), A (m2)	1133	1294	2597	1857
Pressure drop (shell-side), ΔP_s (kPa)	148	149	172	205
Pressure drop (tube-side), ΔP_t (kPa)	105	70	122	13
Shell type	U-shell	U-shell	TEMA E	TEMA F
Baffle type	double-segmental	double-segmental	single-segmental	double-segmental
Total number of shells, N_s (-)	1	1	1	1
Heat exchanger cost, C_{Hx} (k€)	1019	1267	1437	568

Table 5

Proposed design of the heat exchangers for the SG layout with two trains.

Parameter	Superheater	Reheater	Evaporator	Preheater
Shell diameter, D_s (mm)	600	731	1169	1066
Baffle cut, B_c (%)	28	22	28	26
Baffle spacing, L_{bc} (mm)	443	228	470	515
Tubes ext. diameter, D_t (mm)	12.7	25.4	15.9	12.7
Tubes int. diameter, D_{ti} (mm)	9.4	21.2	12.2	9.4
Tube pitch, L_{tp} (mm)	19.0	31.8	19.9	19
Tube layout, θ_{tp} (º)	30	30	30	45
Tube passes, N_{tp} (-)	1	1	2	2
Tubes number, N_{tt} (-)	731	412	1396-U	1088-U
Tube length, L_t (m)	20.19	22.35	9.32	9.71
Shell thickness, t_s (mm)	9.5	12.7	12.7	15.9
Tubesheet thickness, l_{ts} (mm)	146	134	271	207
U-tube minimal radius, R_{min} (mm)	441	849	40	38
Mass flow (tube-side), $\dot{m}_t$ (kg/s)	43.46	39.35	305.37	43.46
Mass flow (shell-side)), $\dot{m}_s$ (kg/s)	195.22	91.65	286.87	286.87
Flow velocity (tube-side), v_t (m/s)	18.70	23.70	2.68	0.76
Flow velocity (shell-side), v_s (m/s)	0.47	0.44	0.50	0.66
Convective heat transfer coefficient (tube-side), h_t (W/m^2 ºC)	5088	1216	28370	8368
Convective heat transfer coefficient (shell-side), h_s (W/m^2 ºC)	4499	3324	3716	4382
Fouling resistance (tube-side), R_t (ºC m^2/W)	8.825e-5	8.825e-5	2.647e-04	8.825e-5
Fouling resistance (shell-side), R_s (ºC m^2/W)	8.825e-5	8.825e-5	8.825e-5	8.825e-5
Overall heat transfer coefficient, U (W/m^2 ºC)	1341	648	1247	1544
Heat exchange area (per shell), A (m2)	524	662	1347	871
Pressure drop (shell-side), ΔP_s (kPa)	146	149	119	199
Pressure drop (tube-side), ΔP_t (kPa)	253	70	133	18
Shell type	U-shell	U-shell	TEMA E	TEMA F
Baffle type	double-segmental	double-segmental	single-segmental	double-segmental
Total number of shells, N_s (-)	2	2	2	2
Heat exchanger cost, C_{Hx} (k€)	1355	1886	1534	509

Table 6
Proposed design of the steam drums

Parameter	One Train	Two Trains
Drum cost, C_{drum} (k€)	201	193
Drum diameter, D_{drum} (mm)	1799	1272
Drum wall thickness, t_{drum} (mm)	111	79.4
Drum length L_{drum} (m)	9.00	6.36
Number of drums, N_{drums} (-)	1	2
Riser diameter, D_r (mm)	150	147
Riser wall thickness, t_r (mm)	6.4	6.4
Number of risers (per drum), N_r (-)	24	13
Downcomers diameter, D_{dc} (mm)	428	445
Downcomers wall thickness, t_{dc} (mm)	6.4	6.4
Number of downcomers (per drum), N_{dc} (-)	2	1

The results show that the SG with one train has lower capital cost than with two trains. Moreover, the start-up energy cost is around 50% lower for the SG with one train. This seems logical since the SG with two trains a larger mass of metal and fluid must be warmed-up. The SG pump operating costs are practically the same for both SG layouts.

Table 4 shows that higher thicknesses are obtained in shells and tubesheets for the SG layout with one train. Since SPTPs plants are subjected to daily start-ups, it is expected that the SG layout with two trains shows a better behavior against thermal stresses. Furthermore, this may lead to lower start-up times when using only one of the two parallel trains due to its lower thermal inertia compared to the SG with one train. This feature could be interesting to increase the plant operability.

5. Conclusions

In this work, the design of the heat exchangers of the steam generator for a 110MWe solar power tower plant is presented. A methodology to optimize the evaporator pinch point temperature difference is proposed considering several costs associated with the performance of the whole system.

An optimization method based on genetic algorithms is also proposed to find economic and feasible heat exchanger designs. This is made following TEMA standards, ASME Pressure Vessel code and the good practice recommendations of several references. A thorough mechanical design is performed considering thermal stresses on tubesheets and U-bends. Furthermore, a vibration analysis is carried out to assure the safe operation.

The cost analysis shows lower annual costs (capital and operation) for the forced circulation evaporator comparing to the natural circulation design. The forced circulation evaporator is also preferred because

this design may lead to shorter start-up times. An approach point temperature difference analysis is carried out in order to avoid subcooled flow boiling in the preheater. Then, lower cost materials could be used in the preheater reducing in this way the capital cost.

The final steam generator design consists of: U-shell design for superheater and reheater, TEMA E shell for evaporator and TEMA F shell for preheater. The TEMA E shell in the evaporator provides a good solution to reduce the thermal stresses in tubesheet and U-tube. Two steam generator layouts are studied: with one or two trains of heat exchangers. The results show that the global optimum of the evaporator pinch points are 2.6 ºC and 3ºC for the steam generator with one and two trains, respectively, while their respective capital cost are 4.3 M€ and 5.3 M€.

Acknowledgements

This work has been supported by the Spanish government under the project ENE2015-69486-R.

Appendix A. Evaporator calculations.

The properties of the two phase flow on the tube side have great changes along the tube length, therefore the evaporator is discretized with $N = N_b$ and $M = N_{tp}$ .The Fig. A1 shows the heat exchanger discretization cell model.

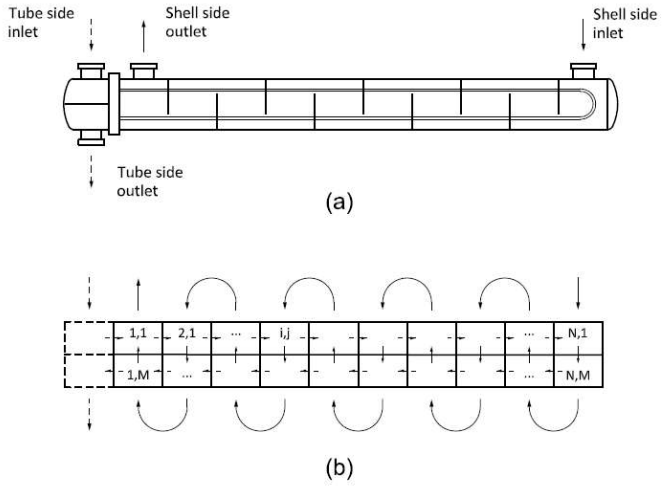

Fig. A1. Heat exchanger discretization cell model.

The energy balance in each cell leads to Equations A1, A2 and A2. In the first step, the two-phase heat transfer coefficient on tube side $h_{t,local}$ and the overall heat transfer coefficient U_{local} are calculated by means of the initial conditions (the inlet salt temperature and the inlet steam quality). Then, the local heat flux, the salt outlet temperature and the outlet steam quality are calculated using Equations A1, A2 and A3. Furthermore, local properties are evaluated in each cell: the two-phase zone ($zone_{tp}$), the critical heat flux (q_{crit}), the two-phase velocity (v_{tp}), the two-phase pressure drop (ΔP_{tp}). The process is repeated until the sum of local heat flux is $\sum \Delta q = Q_{ev}$. Then the evaporator heat transfer area is calculated as: $A = \Delta A \cdot N \cdot M$ and the pressure drop on tube side: $\Delta P_{t,EV} = \sum \Delta P_{tp}$. A schematic of the evaporator calculations is shown in Fig. A2.

$$\Delta q(i,j) = U_{local}(i,j)\,\Delta A(\bar{T}_{sa}(i,j) - T_{sat}) \tag{A1}$$

$$T_{sa,out}(i,j) = \frac{\Delta q(i,j)}{\dot{m}_{sa}\, C_{p,sa}} + T_{sa,in}(i,j) \tag{A2}$$

$$x_{out}(i,j) = x_{in}(i,j) + \frac{\Delta q(i,j)}{h_{fg}\dot{m}_{rec}} \tag{A3}$$

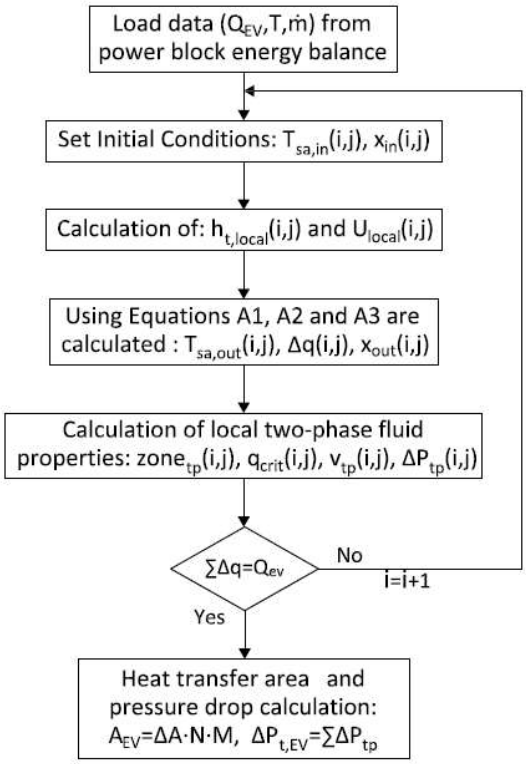

Fig. A2. Scheme of the evaporator calculation.

Appendix B. Tubesheet stress calculations according to O'Donnell et al. [36]**.**

Since ASME Section VIII-Division 1 or/and TEMA standards does not takes into account thermal loads, the method proposed by O'Donnell et al. [36] is used for tubesheet thickness calculation. The main equations for the stress calculations proposed by O'Donnell et al. [36] are shown in Table B1. Also, an schematic of the main tubesheet zones is illustrated in Fig. B1.

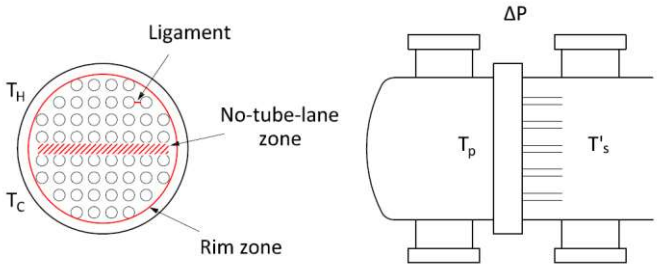

Fig. B1. Schematic of Tubesheet zones.

Table B1
Main equations for stress calculations proposed by O'Donnell et al. [36].

Load	Stress intensity	Equation
Pressure and thermal	Average across ligament at either surface of plate	$\sigma_{eff} = K\frac{R}{h}\lvert\sigma_1\rvert$ (B1)
Pressure	Average across ligament and through thickness	$S_{eff} = \frac{R}{h}\left[\left(\frac{\Delta P r}{H}\right)^2 + (\sigma_r)^2\right]$ (B2)
Pressure and thermal	Peak in ligaments	$\sigma_{max} = Y\sigma_1 + P$ (B3)
Pressure and thermal	Peak at perforations adjacent to rim	$\sigma_{max} = K_r\sigma_{rim} + P$ (B4)
Thermal (skin effect)	Peak at surface	$\sigma_{max} = \frac{E\alpha_T(T_P - T'_s)}{1-\nu}$ (B5)
Thermal (temperature difference across no-tube-lane zone)	Peak in ligaments	$\sigma_{max} = \frac{K_u E^* \alpha_T (T_H - T_C)}{2}$ (B6)
Thermal (temperature difference across no-tube-lane zone)	Peak at holes adjacent to no-tube-lane zone	$\sigma_{max} = \frac{K_D E \alpha_T (T_H - T_C)}{2(1-\nu)}$ (B7)

The calculation process of the tubesheet stresses is described in the following steps:

1. Calculation of the effective elastic constants according to O'Donnell et al. [36].
2. Calculation of the stresses due to the pressure load in an equivalent solid plate in the radial, σ_r^p, and tangential, σ_θ^p directions [51].
3. Calculation of the stress due to the thermal loads using Equation B5 where: $\sigma_\theta^t = \sigma_r^t = \sigma_{skin}$.
4. The stress of an equivalent solid plate, σ_1, is calculated considering only the pressure load where : $\sigma_1 = \max(\lvert\sigma_\theta^p\rvert, \lvert\sigma_r^p\rvert)$. Then, the average stress across ligament at either surface of plate is calculated using Equation B1which must be lower than: $\sigma_{eff} \le 1.5 S_m$.

5. Calculation of the average stress across ligament and through thickness using Equation B2 which must be lower than: $S_{eff} \le S_m$.

6. The stress of an equivalent solid plate, σ_1, is calculated combining pressure and thermal loads where: $\sigma_1 = \max(\left|\sigma_\theta^p + \sigma_\theta^t\right|, \left|\sigma_r^p + \sigma_r^t\right|)$. Then, the average stress across ligament at either surface of plate is calculated using Equation B1 which must be lower than: $\sigma_{eff} \le 3S_m$.

Appendix C. U-Tube stress calculations according to Singh et al. [36].

Based on the elasticity theory, the energy deformation of the tubes in the straight and curve sections can be calculated as follows:

$$U = \int \frac{N^2}{2EA} ds + \int \frac{V^2}{2GA} ds + \int \frac{M^2}{2EI} ds \tag{C1}$$

The forces and displacements can be related using Castigliano's theorem:

$$\frac{\partial U}{\partial P} = u; \qquad \frac{\partial U}{\partial R} = v; \qquad \frac{\partial U}{\partial M} = \alpha; \tag{C2}$$

Then, the moment on a generic point (M_i) can be written as function of the stiffness K_i and the rotation angle α_i as: $M_i = K_i \alpha_i$. The stiffness is expressed as function of $K_i = f(\alpha_i, L, L_{bc}, E, I)$. Since the rotation angles (α_i) are unknown, initial values must be set for the stiffness calculation (K_i^0), and then the matrix $[B]$ can be calculated. The rotation angle (α_2), the vertical force (R) and the axial force (P) in leg 2 are calculated as follows:

$$\begin{Bmatrix} \alpha_2 \\ R \\ P \end{Bmatrix} = [B]^{-1} \begin{Bmatrix} \delta \\ 2\Delta - \varepsilon_1 - \varepsilon_2 \\ 0 \end{Bmatrix} \tag{C3}$$

where δ is free thermal expansion of leg1 over leg 2, Δ is the increase in the radius of the U-bend due to its temperature rise, ε_1 and ε_2 are the vertical displacements of leg 1 and 2, respectively. The rotation angle in leg 1 is calculated by means of the moment equilibrium on U-bend:

$$\alpha_1 = \frac{1}{K_1^0}(K_2^0\alpha_2 + 2Pr - R(S_1 - S_2)) \tag{C4}$$

where r is the U-bend radius, S_1 and S_2 are the overhang longitudes. At this point, the rotation angles are known, and then the values of stiffness can be recalculated obtaining K_i^1. The process is repeated until the convergence of stiffness values is achieved: $\Delta K_i = K_i^1 - K_i^0 \leq tol$. Once the problem is converged, the stress on the U-bend is calculated as follows:

$$M(\theta) = M_2 + R(S_2 + r\sin\theta) + Pr(1-\cos\theta) \tag{C5}$$

$$\sigma(\theta) = \frac{\psi\ M(\theta)\ C_o}{I} \tag{C6}$$

where ψ is the stress intensification factor for the U-bend and C_o is the outer tube radius.

References

[1] Sandia Natl. Lab., Molten Salt Receiver Subsystem Research Experiment Phase 1 - Final Report, Volume 1. Foster Wheeler Solar Development Corporation, Sandia Natl. Lab. Report SAND82-8179, (1984).

[2] Sandia .Natl. Lab., Betchel. Corporation, Investigation of Thermal Storage and Steam Generator Issues, Sandia Natl. Lab. Report SAND 93-7084, (1993).

[3] J.E. Pacheco, Final Test and Evaluation Results from the Solar Two Project, Sandia Natl. Lab. Report, SAND2002-0120, (2002).

[4] W. a. Allman, D.C. Smith, C.R. Kakarala, The Design and Testing of a Molten Salt Steam

Generator for Solar Application, J. Sol. Energy Eng. 110 (1988) 38–44. doi:10.1115/1.3268235.

[5] A.B. Zavoico, Solar Power Tower - Design Basis Document, Sandia Natl. Lab. Report, SAND2001-2100, (2001).

[6] B. Kelly, Lessons Learned, Project History, and Operating Experience of the Solar Two Project, Sandia Natl. Lab. Report SAND2000-2598, 1 (2000).

[7] R. Moore, M. Vernon, C.K. Ho, N.P. Siegel, G.J. Kolb, Design considerations for concentrating solar power tower systems employing molten salt, Sandia Natl. Lab. Report, SAND2010-6978, (2010).

[8] G.J. Kolb, An Evaluation of Possible Next-Generation High-Temperature Molten-Salt Power Towers, Sandia Natl. Lab. Report, SAND2011-9320, (2011).

[9] B. Kelly, Advanced Thermal Energy Storage for Central Receivers with supercritical coolants, Abengoa Solar Inc., (2010).

[10] A.C. Caputo, P.M. Pelagagge, P. Salini, Heat exchanger design based on economic optimisation, Appl. Therm. Eng. 28 (2008) 1151–1159. doi:10.1016/j.applthermaleng.2007.08.010.

[11] H. Sadeghzadeh, M.A. Ehyaei, M.A. Rosen, Techno-economic optimization of a shell and tube heat exchanger by genetic and particle swarm algorithms, Energy Convers. Manag. 93 (2015) 84–91. doi:10.1016/j.enconman.2015.01.007.

[12] H. Hajabdollahi, P. Ahmadi, I. Dincer, Thermoeconomic optimization of a shell and tube condenser using both genetic algorithm and particle swarm, Int. J. Refrig. 34 (2011) 1066–1076. doi:10.1016/j.ijrefrig.2011.02.014.

[13] P.A. González-Gómez, F. Petrakopoulou, J.V. Briongos, D. Santana, Cost-based design optimization of the heat exchangers in a parabolic trough power plant, Energy. 123 (2017) 314–325.

[14] National Renewable Energy Laboratory (NREL), (2016). http://www.nrel.gov/csp/solarpaces/by_project.cfm.

[15] W.J. Garland, B.J. Hand, Simple Functions for the Fast Approximation of Light Water Thermodynamic Properties, Nucl. Eng. Des. 113 (1989) 21--34. doi:http://dx.doi.org/10.1016/0029-5493(89)90293-8.

[16] National Renewable Energy Laboratory (NREL), Solar Advisor Model Reference Manual for CSP Trough Systems, (2009).

[17] G.P. Purohit, Estimating costs of shell-and-tube heat exchangers, Chem. Eng. (1983) 56–67.

[18] A. Pasha, Gas Turbine Heat Recovery Steam Generators for Combined Cycles Natural or Forced Circulation Considerations, ASME 1988 International Gas Turbine and Aeroengine Congress and Exposition, Volume 4: Heat Transfer; Electric Power; Industrial and Cogeneration, , (1988).

[19] V. Ganapathy, Understanding Boiler Circulation, Chem. Eng. (2013) 52–56.

[20] J.W. Palen, Shell and Tube Reboilers. In Heat Exchanger Design Handbook, Hemisph. Publ. Corp. (1983).

[21] W. Francis, M.C. Peters, Fuels and Fuel Technology, Reg. Oceanogr. (1980).

[22] V. Ganapathy, Heat-recovery steam generators: Understand the basics, Chem. Eng. Prog. 92 (1996) 32–45.

[23] V. Ganapathy, Steam Generators and Waste Heat Boilers: For Process and Plant Engineers, (2015).

[24] R.W. Serth, T.G. Lestina, Process Heat Transfer: Principles, Applications and Rules, (2014).

[25] ESDU, Engineering Science Data Unit (ESDU), Baffled Shell-and-Tube Heat Exchangers: Flow Distribution, Pressure Drop and Heat Transfer Coefficient on the Shellside, Item No. 83038, (1984).

[26] R. Shah, D. Sekulic, Fundamentals of Heat Exchangers Design, John Wiley & Sons Inc., (2003).

[27] K.P. Singh, M. Holtz, A Method to Design Shell-Side Pressure Drop Constrained Tubular Heat Exchangers, Eng. Power. (1977) 441–448.

[28] W.H. Emerson, Shell-side pressure drop and heat transfer with turbulent flow in segmentally baffled shell-and-tube heat exchangers, Int. J. Heat Mass Transf. 6 (1963) 649–668. doi:10.1016/0017-9310(63)90037-1.

[29] J.C. Chen, Correlation for boiling heat transfer to saturated fluids in convective flow, Ind. Eng. Chem. Process Des. Dev. 5 (1966) 322–329. doi:10.1021/i260019a023.

[30] J.G. Collier, J.R. Thome, Convective Boiling and Condensation, Clarendon Press, (1994).

[31] Y.L. Wong, D.C. Groeneveld, S.C. Cheng, Chf prediction for horizontal tubes, Int. J. Multiph. Flow. 16 (1990) 123–138. doi:10.1016/0301-9322(90)90043-I.

[32] G.R. Warrier, V.K. Dhir, Heat Transfer and Wall Heat Flux Partitioning During Subcooled Flow Nucleate Boiling--A Review, J. Heat Transfer. 128 (2006) 1. doi:10.1115/1.2349510.

[33] I.S. Hussaini, S.M. Zubair, M.A. Antar, Area allocation in multi-zone feedwater heaters, Energy Convers. Manag. 48 (2007) 568–575. doi:10.1016/j.enconman.2006.06.003.

[34] TEMA Report, Standards of the Tubular Exchangers Manufacturers Association, (2007).

[35] American Society of Mechanical Engineers. ASME boiler and pressure vessel code, Section VIII, (2010).

[36] W.J. O'Donnell, B.F. Langer, Design of perforated plates, J. Eng. Ind. 84 (1962) 307–319. doi:10.1115/1.3667483.

[37] J. Busuttil, Detailed stress analysis of SM-1 steam generator tube sheet, ALCO Products Inc., (1962).

[38] K.P. Singh, M. Holtz, On Thermal Expansion Induced Stresses in in U-Bends of Shell-and- Tube Heat Exchangers, Eng. Power. 101 (1979) 634–639.

[39] J. Taborek, Shell and Tube Heat Exchangers: single phase flow. In Heat Exchanger Design Handbook, Hemisph. Publ. Corp. (1983).

[40] ESDU, Engineering Science Data Unit (ESDU), Flow induced vibration in tube bundles with

particular reference to shell and tube heat exchangers, Item No. 87019, (1987).

[41] U. Vengateson, Design of multiple shell and tube heat exchangers in series: E shell and F shell, Chem. Eng. Res. Des. 88 (2010) 725–736. doi:10.1016/j.cherd.2009.10.005.

[42] W.D. Seider, J.D. Seader, D.R. Lewin, S. Widagdo, Product and process design principles: synthesis, analysis, and evaluation, (2010).

[43] B. Kelly, D. Kearney, Thermal Storage Commercial Plant Design Study for a 2-Tank Indirect Molten Salt System Final Report, (2006).

[44] M.R. Rodriguez-Sanchez, A. Sanchez-Gonzalez, C. Marugan-Cruz, D. Santana, Saving assessment using the PERS in solar power towers, Energy Convers. Manag. 87 (2014) 810–819. doi:10.1016/j.enconman.2014.07.076.

[45] J. Yang, A. Fan, W. Liu, A.M. Jacobi, S.-R.R. Oh, W. Liu, Optimization of shell-and-tube heat exchangers conforming to TEMA standards with designs motivated by constructal theory, Energy Convers. Manag. 77 (2014) 468–476. doi:10.1016/j.ijheatmasstransfer.2014.06.046.

[46] J.M. Ponce-Ortega, M. Serna-González, A. Jiménez-Gutiérrez, Use of genetic algorithms for the optimal design of shell-and-tube heat exchangers, Appl. Therm. Eng. 29 (2009) 203–209. doi:10.1016/j.applthermaleng.2007.06.040.

[47] M. Ghazi, P. Ahmadi, A.F. Sotoodeh, A. Taherkhani, Modeling and thermo-economic optimization of heat recovery heat exchangers using a multimodal genetic algorithm, Energy Convers. Manag. 58 (2012) 149–156. doi:10.1016/j.enconman.2012.01.008.

[48] M. Čehil, S. Katulić, D.R. Schneider, Novel method for determining optimal heat-exchanger layout for heat recovery steam generators, Energy Convers. Manag. (2017). doi:10.1016/j.enconman.2017.03.033.

[49] Energetica Int., Lebrija 1 : International solar thermal reference, (2012).

[50] C. A. D. Andalucía, 43.321/05. Solicitud de aprobación del proyecto de ejecución, y declaración en concreto de la utilidad pública del proyecto Andasol-1, (2005).

[51] S. Timoshenko, Theroy of Plates and Shells, McGraw-Hill Book Co., (1940).

List of Figures

List of Tables